

# HARP: Hadamard-Preconditioned Adaptive Rotation Processor for Extreme LLM Quantization

Artur Zagitov  
BRAIn Lab  
Moscow, Russia

Gleb Molodtsov  
BRAIn Lab  
Moscow, Russia

Aleksandr Beznosikov  
BRAIn Lab  
Moscow, Russia

## Abstract

Post-training quantization (PTQ) is essential for deploying LLMs under memory and bandwidth constraints. However, extreme low-bit quantization remains highly sensitive to activation outliers and anisotropic weight curvature. Existing incoherence-based PTQ methods mitigate this issue with fixed randomized Hadamard transforms (RHTs), which improve quantization robustness but cannot adapt the rotated basis to the layer, calibration distribution, or quantizer. We introduce HARP (**H**adamard-**p**reconditioned **A**daptive **R**otation **P**rocessor), a learnable structured two-sided orthogonal processor that replaces fixed Hadamard mixing while preserving exact full-precision equivalence. HARP represents each rotation as a product of sparse butterfly-like block-orthogonal stages, supports non-power-of-two dimensions via Mixed-Radix schedules, and initializes to the RHT processor up to a fixed permutation. Fitted only on calibration data, HARP adapts the quantization basis to each layer and backend. Across 2-4 bit settings on models ranging from 1B to 70B parameters, HARP improves perplexity and zero-shot accuracy over fixed RHT. Importantly, HARP preserves deployment efficiency, reaching 128 tok/s versus 61 tok/s for FP16.

## 1 Introduction

Large language models (LLMs) have become central to modern NLP, yet their scale makes deployment increasingly constrained by memory bandwidth. During inference, repeated weight and activation transfers through the memory hierarchy dominate latency and serving cost. Quantization targets this bottleneck by compressing weights and activations to fewer bits.

Post-training quantization (PTQ) is especially attractive because it operates on a fixed pretrained model, uses only a small calibration set, and avoids the expense of full training (Frantar et al., 2022;

Xiao et al., 2023; Lin et al., 2024; Shao et al., 2023). Successful PTQ pipelines do more than choose a rounding rule; they are defined by several coupled design choices, including calibration, representation preprocessing, the reconstruction objective, and the code family used for compression.

In the extreme low-bit regime, outlier handling becomes central. At such bitwidths, small reconstruction errors are amplified across many layers, and heavy-tailed statistics make the quantization problem substantially harder. As a result, this preprocessing can fundamentally change the difficulty of the quantization problem by reshaping the coordinates in which quantization is performed.

Incoherence processing exploits this degree of freedom by applying structured orthogonal changes of basis before quantization. The full-precision layer remains unchanged, but weight mass and curvature-sensitive directions are spread across coordinates, making them less aligned with a few outlier axes (Chee et al., 2023). In practice, randomized Hadamard transforms (RHTs) have become the default preprocessing choice because they are exactly orthogonal, fast, and admit simple  $O(d \log d)$  kernels (Tseng et al., 2024a,b).

Although the standard Hadamard/RHT processor provides a strong generic mixing basis, it does not adapt to the layer, the calibration distribution, and the block structure of the downstream quantizer. Meanwhile, recent evidence shows that the choice of rotation is not incidental: end-to-end rotation methods reveal substantial variation across rotations and motivate learning them from data (Ashkboos et al., 2024b; Liu et al., 2024b), while closed-form data-aware transforms can improve over fixed Hadamard mixing under specific quantizer assumptions (Chen et al., 2025). These alternatives, however, often target different operating points, relax the drop-in structure of Hadamard-based PTQ, or introduce rotations that are too costly to use. This leaves a gap: the preprocessing

module should be learnable from calibration data, remain an exact orthogonal change of basis, and preserve the Hadamard-like efficiency that makes incoherence processing practical.

We present HARP (**H**adamard-**p**reconditioned **A**daptive **R**otation **P**rocessor), a learnable two-sided orthogonal processor for extreme low-bit PTQ. HARP satisfies three requirements simultaneously: (i) adaptivity, by fitting rotations to each layer and quantizer backend; (ii) faithfulness, by remaining an exact change of basis that preserves the full-precision model; and (iii) efficiency, by using staged butterfly-like block-orthogonal factors instead of dense rotations. Crucially, HARP is drop-in compatible with existing Hadamard-based PTQ pipelines: at initialization, it recovers the RHT processor up to a fixed permutation convention, after which calibration learns a structured orthogonal refinement around this strong baseline.

### Contributions.

Our main contributions are:

- We introduce HARP, a learnable two-sided orthogonal incoherence processor for PTQ that is fit using only calibration data and compatible with both scalar and vector-quantized backends.
- We design HARP as a drop-in replacement for fixed RHT/Hadamard preprocessing: at initialization, it recovers the randomized Hadamard processor up to a fixed permutation, and calibration learns a structured orthogonal refinement.
- We demonstrate consistent quality gains over fixed RHT across 2-4 bit settings on models from 1B to 70B parameters while retaining most of the RHT throughput advantage via a hardware-aware optimization. Our code is open-sourced<sup>1</sup>.

## 2 Setup

**Layerwise PTQ objective.** Modern PTQ pipelines typically cast quantization as a layerwise reconstruction problem.

We consider PTQ of a linear layer with  $W \in \mathbb{R}^{d_{\text{out}} \times d_{\text{in}}}$  and calibration inputs  $x \in \mathbb{R}^{d_{\text{in}}}$ . As in Hessian-aware PTQ, we use the empirical second moment as a curvature proxy:

$$H := \mathbb{E}[xx^\top] \in \mathbb{R}^{d_{\text{in}} \times d_{\text{in}}}. \quad (1)$$

Given that, PTQ seeks an approximation  $\widehat{W}$  constrained to a code family  $\mathcal{Q}$  that minimizes a proxy for the output error. Scalar quantization rounds weights independently, which is simple and kernel-

friendly but can be inefficient at very low bitwidths. Vector quantization (VQ) instead quantizes small blocks jointly using a structured code family. By shaping quantization noise in a higher-dimensional space, VQ can significantly reduce distortion at a fixed bitrate, but it introduces more complex encoding/decoding and raises hardware considerations for fast inference. A common choice is a second-moment or Hessian-weighted quadratic objective, which captures how errors along different input directions affect the layer output.

$$\mathcal{L}(W, \widehat{W}) := \text{Tr}\left((W - \widehat{W})H(W - \widehat{W})^\top\right). \quad (2)$$

This perspective yields scalable algorithms because it allows optimization independently per layer (and often per block within a layer), using tractable curvature approximations derived from calibration activations (Frantar et al., 2022; Hassibi and Stork, 1992; Hassibi et al., 1993; Wu et al., 2024; Frantar and Alistarh, 2022).

**Incoherence Processing for PTQ.** Extreme low-bit PTQ is often dominated by anisotropy and outliers: a small subset of coordinates can carry disproportionate mass in  $W$  and in the curvature proxy  $H$ . This harms blockwise quantizers because their scales and code assignments must cover rare directions, reducing effective resolution for the majority of weights.

Incoherence processing addresses this by applying an orthogonal change of basis so that energy is less concentrated in a few coordinates. For a linear layer, we choose two orthogonal processors  $U \in O(d_{\text{out}})$  and  $V \in O(d_{\text{in}})$ , rotate the weight and curvature proxy as

$$\widetilde{W} := U^\top W V, \quad \widetilde{H} := V^\top H V.$$

The backend then quantizes the rotated weight, producing  $\widehat{\widetilde{W}}$ , and the quantized layer is mapped back to the original basis as  $\widehat{W} := U \widehat{\widetilde{W}} V^\top$ . Because  $U$  and  $V$  are orthogonal, cyclicity of trace gives the invariant reconstruction objective

$$\mathcal{L}(W, \widehat{W}) = \text{Tr}\left((\widetilde{W} - \widehat{\widetilde{W}}) \widetilde{H} (\widetilde{W} - \widehat{\widetilde{W}})^\top\right). \quad (3)$$

Thus, the full-precision layer and the target reconstruction objective are unchanged; only the basis exposed to the finite-code quantizer changes.

This is particularly important because low-bit quantizers are generally not invariant to rotations. Scalar quantizers are axis-aligned, and blockwise VQ backends operate on fixed contiguous groups. If large weights or curvature-sensitive directions align with a few coordinates, scales and code as-

<sup>1</sup><https://github.com/brain-lab-research/HARP>

signments must cover rare outliers, reducing resolution for the majority of values. Randomized Hadamard transforms (RHTs) reduce this concentration generically. HARP keeps the same orthogonal reparameterization principle, but learns a structured rotation that adapts to the layer and downstream blockwise quantizer.

Following QuIP, one can measure generic concentration using weight incoherence

$$\mu_W(A) := \sqrt{mn} \frac{\|A\|_\infty}{\|A\|_F}, \quad A \in \mathbb{R}^{m \times n}, \quad (4)$$

and Hessian incoherence

$$\mu_H(H) := \sqrt{n} \|Q\|_\infty, \quad H = Q\Lambda Q^\top. \quad (5)$$

Lower values indicate that weights or curvature-sensitive directions are less concentrated in a few coordinate axes. Classical incoherence scores are useful but not sufficient for modern blockwise quantizers. A rotation can reduce outliers while still misaligning curvature with the quantizer’s blocks, or conversely increase a generic Hessian incoherence score while producing lower backend-specific reconstruction error. For this reason, we evaluate both classical metrics and quantizer-aligned diagnostics in Appendix E: pre-quantization weight incoherence, quantized-weight incoherence, off-block Hessian energy, diagonal Hessian-weighted distortion, and classical Hessian incoherence. The diagnostics show HARP does not simply optimize every generic incoherence score; rather, it learns a basis that is more favorable for the deployed blockwise quantizer.

Fixed randomized Hadamard transforms (RHT) are a popular choice because they are orthogonal and fast. However, they ignore per-layer statistics and quantizer structure. HARP keeps Hadamard-like efficiency and exact orthogonality while learning a structured refinement from calibration data.

### 3 HARP processors: structured orthogonal rotations

A dense learned rotation would be too expensive to store or apply at LLM hidden dimensions. HARP therefore parameterizes each processor as a product of sparse stride stages, following the same high-level structure as fast Hadamard and butterfly transforms. Fix a transformed dimension  $d$  (either  $d_{\text{in}}$  or  $d_{\text{out}}$ ) and choose a Mixed-Radix schedule

$$\mathbf{b} = (b_0, \dots, b_{m-1}), \quad b_t \geq 2, \quad (6)$$

$$\prod_{t=0}^{m-1} b_t = d.$$

The schedule determines which coordinates are mixed at each stage. In all experiments we use a greedy schedule with preferred radix 8; Appendix J.2 gives the construction and Appendix F.1 ablates the radix choice.

At stage  $t$ , define the stride  $s_t := \prod_{j < t} b_j$  and the number of blocks  $D_t := d/b_t$ . Conceptually, a perfect-shuffle permutation  $P_t$  groups the  $b_t$  coordinates mixed by stage  $t$  into contiguous blocks. The stage operator is

$$S_t(\Theta_t) := P_t^\top \mathcal{B}_t(\Theta_t) P_t, \quad (7)$$

$$\mathcal{B}_t(\Theta_t) := \text{BlkDiag}(B_{t,1}, \dots, B_{t,D_t}),$$

where each  $B_{t,c} = B_{t,c}(\theta_{t,c}) \in \mathbb{R}^{b_t \times b_t}$  is orthogonal. The one-pass HARP transform is

$$T(\Theta) := S_{m-1}(\Theta_{m-1}) \cdots S_0(\Theta_0). \quad (8)$$

Since each stage is orthogonal,  $T(\Theta)$  is orthogonal. Multiple passes can be used by composing independent copies of the same schedule, although we use one pass by default.

Although Eq. (7) is written with a permutation, no explicit gather is used. The input is reshaped to expose the stride- $s_t$  groups, transposed so that each length- $b_t$  group is contiguous, multiplied by the corresponding block kernel, and reshaped back. This preserves the staged execution pattern that makes Hadamard preprocessing efficient. Appendix J.1 gives an index-view example of the stride layout.

HARP uses independent processors for the input and output sides, giving the rotations  $V$  and  $U$  used in Eq. (3). As in RHT preprocessing, we also include diagonal Rademacher sign flips. In our QuIP# integration, these signs are already part of the pipeline; HARP reuses them and replaces only the fixed Hadamard mixing component.

#### 3.1 Hadamard-preconditioned block kernels and initialization

HARP uses block kernels of the form

$$B_{t,c}(\theta_{t,c}) := Q_{t,c}(\theta_{t,c}) G_{b_t}, \quad (9)$$

where  $Q_{t,c}(\theta_{t,c}) \in SO(b_t)$  is learnable and  $G_{b_t}$  is a fixed orthogonal base mixer. For power-of-two radices,  $G_{b_t}$  is the normalized Sylvester Hadamard matrix  $H_{b_t}$ . For non-power-of-two radices, we use a deterministic orthogonal fallback computed by QR factorization of a fixed Gaussian matrix. Thus  $G_{b_t}^\top G_{b_t} = I$ , so every block remains orthogonal.

Hadamard preconditioning serves two purposes. First, it anchors HARP to a strong baseline: at  $\Theta = 0$ , all learnable blocks satisfy  $Q_{t,c}(0) = I$ ,

so  $B_{t,c}(0) = G_{b_t}$ . For power-of-two schedules, the staged product therefore recovers Hadamard-family preprocessing up to a fixed permutation convention, so HARP is a drop-in upgrade for Hadamard-based incoherence processing pipelines. Second, it makes fitting easier in practice: rather than learning mixing from scratch, HARP learns a structured residual around an already useful incoherence processor, which is helpful when the quantizer objective is highly non-smooth at extreme bitwidths. Appendix F.2 ablates the base mixer choice.

### 3.2 Exact initialization: $\Theta = 0$ recovers RHT

HARP initializes all learnable parameters to zero, so  $Q_{t,c}(0) = I_{b_t}$  and  $B_{t,c}(0) = G_{b_t}$  for every stage  $t$  and block  $c$ . With Hadamard base mixers, the stride stages therefore recover Hadamard-family preprocessing exactly, up to the fixed permutation induced by the reshape convention. Under the same Kronecker fallback used by QuIP# for non-power-of-two dimensions, the initialization also matches QuIP#'s convention. Thus, before calibration, HARP is numerically equivalent to the existing RHT processor up to implementation-level floating-point differences.

**Assumption 1** (Exact RHT equivalence conditions). For each transformed dimension, the following conditions hold:

- (i) For a transformed dimension  $d$ , either: (a)  $d = 2^L$  with a power-of-two stride schedule, or (b)  $d = K \cdot 2^L$  with the Kronecker fallback  $T_d(\Theta)$  from Eq. (12).
- (ii) For every power-of-two stage radix  $b_t$ , the base mixer is the normalized Sylvester Hadamard  $G_{b_t} = H_{b_t}$ .
- (iii) Initialization is exact:  $Q_{t,c}(0) = I_{b_t}$ , hence  $B_{t,c}(0) = G_{b_t}$ .
- (iv) Random sign flips use the same Rademacher signs and placement as the corresponding RHT processor:  $S_U \in \{\pm 1\}^{d_{\text{out}}}$  and  $S_V \in \{\pm 1\}^{d_{\text{in}}}$  are applied as diagonal matrices.

**Theorem.** *Under Assumption 1, HARP at  $\Theta = 0$  implements QuIP#'s randomized Hadamard incoherence processor exactly up to the same fixed permutation convention. With the inherited random signs, the full two-sided processor is the corresponding RHT. Proof in Appendix A.*

### 3.3 Orthogonal parameterization

For  $b_t = 2$ , we use a Givens rotation:

$$Q(\theta) = \begin{bmatrix} \cos \theta & -\sin \theta \\ \sin \theta & \cos \theta \end{bmatrix}. \quad (10)$$

For  $b_t > 2$ , we use the Cayley map. If  $A(\theta) \in \mathbb{R}^{b_t \times b_t}$  is skew-symmetric, then

$$Q(\theta) := (I + A(\theta))^{-1}(I - A(\theta)) \quad (11)$$

is orthogonal whenever  $I + A(\theta)$  is invertible. In implementation,  $A(\theta)$  is obtained by antisymmetrizing an unconstrained tensor.

### 3.4 Mixed-Radix dimensions and Kronecker fallback

The Mixed-Radix schedule in Eq. (6) supports non-power-of-two dimensions directly. For example, 5120 is handled by the schedule (8, 8, 8, 5, 2), using Hadamard mixers for the power-of-two stages and the QR fallback for the radix-5 stage. This avoids padding while preserving exact orthogonality and staged execution.

We also support an optional Kronecker fallback that aligns the initialization more closely with QuIP#'s Hadamard convention and reduces the number of learnable parameters. If  $d = K \cdot n_2$  with  $n_2 = 2^L$ , and a Hadamard-like table  $\tilde{H}_K \in \{\pm 1\}^{K \times K}$  satisfies  $\tilde{H}_K \tilde{H}_K^\top = KI$ , we define

$$T_d(\Theta) := \left( \frac{1}{\sqrt{K}} \tilde{H}_K \right) \otimes T_{n_2}(\Theta). \quad (12)$$

Operationally, this reshapes a vector into a  $K \times n_2$  tensor, applies HARP along the power-of-two axis, and mixes the  $K$  rows with the fixed Hadamard-like table. Mixed-Radix HARP is more general and expressive; the Kronecker fallback is useful when closer compatibility or lower overhead is desired.

### 3.5 Implementation details

#### 3.5.1 Memory and compute

A dense learned orthogonal matrix in  $\mathbb{R}^{d \times d}$  requires  $\Theta(d^2)$  storage and application cost, which is infeasible at LLM hidden dimensions. HARP instead uses  $m$  sparse block stages. For a stage with radix  $b_t$ , there are  $D_t = d/b_t$  blocks, each with  $b_t(b_t - 1)/2$  degrees of freedom, so the parameter count is

$$D_t \frac{b_t(b_t - 1)}{2} = d \frac{b_t - 1}{2}. \quad (13)$$

With bounded radices, this is  $\mathcal{O}(dm)$  parameters per pass. The application cost is  $\mathcal{O}(D_t b_t^2) = \mathcal{O}(d b_t)$  per stage and  $\mathcal{O}(\sum_t d b_t)$  overall, i.e., Hadamard-like  $\mathcal{O}(d \log d)$  for constant radices. This gives learnable exact orthogonal mixing at structured-transform cost.

---

**Algorithm 1** HARP transform  $y = xT(\Theta)$ 

---

**Require:** Input  $x \in \mathbb{R}^{B \times d}$ , stage radices  $(b_0, \dots, b_{m-1})$  with  $\prod_t b_t = d$

**Require:** Fixed base mixers  $G_{b_t} \in \mathbb{R}^{b_t \times b_t}$  and learnable parameters  $\Theta = \{\theta_{t,c}\}$

- 1:  $y \leftarrow x$
  - 2: Precompute strides  $s_t := \prod_{r < t} b_r$  for  $t = 0, \dots, m - 1$
  - 3: **for**  $t = 0$  to  $m - 1$  **do**
  - 4:    $s \leftarrow s_t, \quad g \leftarrow d / (b_t s)$
  - 5:   Reshape  $y$  to  $Y \in \mathbb{R}^{B \times g \times b_t \times s}$
  - 6:   Transpose to  $\hat{Y} \in \mathbb{R}^{B \times g \times s \times b_t}$
  - 7:   Construct block kernels  $K_t \in \mathbb{R}^{(d/b_t) \times b_t \times b_t}$ :  $K_t[c] \leftarrow Q(\theta_{t,c}) G_{b_t}$
  - 8:   View  $K_t$  as  $\mathbb{R}^{g \times s \times b_t \times b_t}$
  - 9:   Apply blockwise multiplication along the last dimension
  - 10:   Invert transpose and reshape back to  $y \in \mathbb{R}^{B \times d}$
  - 11: **end for**
  - 12: **return**  $y$
- 

### 3.5.2 Parameter quantization for deployment

After fitting, we optionally store HARP parameters in int8 form. For each block, we quantize either the Givens angle or the upper-triangular entries of the Cayley matrix using a per-block scale, and reconstruct the corresponding orthogonal block at runtime. This reduces processor storage with little effect on perplexity in our experiments. Appendix J.4 gives the exact packing rule.

### 3.5.3 Fitting HARP processors for PTQ

HARP is fit per layer using calibration statistics and a fixed quantizer backend. Let

$$\begin{aligned}\tilde{W}(\Theta) &= U(\Theta_U)^\top W V(\Theta_V), \\ \tilde{H}(\Theta) &= V(\Theta_V)^\top H V(\Theta_V).\end{aligned}$$

Directly optimizing the full proxy loss in Eq. (3) inside the QuIP# solver would be expensive: it would require repeated multiplication by  $\tilde{H}(\Theta)$  and repeated blockwise second-order quantization steps. We therefore optimize a lightweight surrogate that is cheap enough to evaluate during calibration while remaining aligned with the deployed codebook quantizer.

QuIP# ultimately refines blockwise code assignments using an  $LDL^\top$  factorization of the curvature proxy. During HARP fitting, we do not nest this LDLQ procedure inside the optimizer. Instead, for the current rotated weight we compute a direct blockwise codebook target and treat it as stopped-gradient. This gives a practical training signal: a useful rotation should make  $\tilde{W}$  easier for the downstream code family to represent, especially in curvature-important directions.

Let  $\Delta(\Theta) := \tilde{W}(\Theta) - Q(\tilde{W}(\Theta))$ ,  $w_j(\Theta) := |\tilde{H}_{jj}(\Theta)|$ , and let  $\tilde{w} = w / \text{mean}(w)$ . Our diagonal

Hessian-weighted reconstruction proxy is

$$\mathcal{L}_{\text{diag}}(\Theta) := \frac{1}{d_{\text{out}} d_{\text{in}}} \sum_{i=1}^{d_{\text{out}}} \sum_{j=1}^{d_{\text{in}}} \Delta_{ij}(\Theta)^2 \tilde{w}_j. \quad (14)$$

We stop gradients through  $Q(\tilde{W})$ , so gradients update the rotation parameters through  $\tilde{W}(\Theta)$  rather than through discrete code-assignment changes. This is more stable than straight-through gradients through sharp codebook search.

To better align the rotated curvature proxy with blockwise quantization, we also penalize off-block Hessian energy:

$$\mathcal{R}_{\text{bd}}(\Theta_V) := \frac{1}{d_{\text{in}}^2} \sum_{\substack{p,q \\ p \neq q}} \|\tilde{H}_{pq}\|_F^2. \quad (15)$$

where  $\tilde{H}_{pq}$  denotes a block under the quantizer’s contiguous partition. This term gives  $V$  a direct signal to make curvature more local in the same block structure used by the backend. The total fitting loss is

$$\mathcal{L}_{\text{fit}}(\Theta) := \mathcal{L}_{\text{diag}}(\Theta) + \lambda_{\text{bd}} \mathcal{R}_{\text{bd}}(\Theta_V). \quad (16)$$

We optimize  $\Theta_U, \Theta_V$  with Adam from the exact RHT initialization. Appendix J.3 gives the full layerwise fitting procedure, including the target-refresh variant used to reduce calibration time.

## 4 Experiments

**Scope of comparison.** Our primary experimental comparison isolates a single component: the incoherence processor inside a fixed QuIP#-style backend. We therefore compare HARP directly against RHT under the same backend, and separately report context-matched comparisons to published AWQ, GPTQ, OmniQuant, and SpinQuant results where the evaluation protocols are compatible. We also include a QTIP experiment to test whether the same learned processor can be inserted into a distinct RHT-based PTQ backend.

**Models.** We report results on Llama 3.2 (1B, 3B) and Llama 2 (7B, 13B, 70B).

**No-finetuning comparison.** Our main tables intentionally compare quantization *without* QuIP#’s weight fine-tuning stages. This isolates the effect of replacing the fixed RHT mixer with HARP: the codebooks, solver, signs, calibration statistics, and evaluation harness are kept fixed. This choice should not be read as an incompatibility with fine-tuning. Appendix H shows that HARP can be combined with QuIP#’s fine-tuning-during-quantization stage, and that HARP with only this stage already improves over the RHT setting.

**Evaluation protocol.** We report perplexity (PPL, ↓) on Wikitext2 and C4. For Llama 3.2 models, we use context length 8192. For Llama 2 models in the main QuIP#-style table, we use context length 4096, matching the Llama 2 context used in QuIP# comparisons. To compare against AWQ/GPTQ/OmniQuant-style baselines, we additionally report Llama 2 results at context length 2048 in Table 5, since those papers commonly use this context. We evaluate zero-shot accuracy using `lm_eval` and report `acc` (not `acc_norm`) on ARC-Challenge, ARC-Easy, PIQA, and WinoGrande.

**Methods compared.** *FP16* is the unquantized baseline. *RHT* uses fixed randomized Hadamard preprocessing as in QuIP#. Unless explicitly attached to another backend (e.g., QTIP+HARP), *HARP* denotes the same QuIP# backend with its fixed Hadamard mixer replaced by learned HARP processors. HARP keeps the same random sign flips, codebooks, solver, and evaluation pipeline. Unless explicitly stated, HARP uses the Mixed-Radix variant. For 2-bit experiments we additionally report the Kronecker fallback.

**Effective bitrate accounting.** We report effective bits-per-parameter (BPP) assuming the underlying quantized weights contribute exactly the nominal bitrate and adding storage overhead from HARP processor parameters and metadata. RHT is therefore reported at exactly the nominal bitrate. We report both floating-point HARP parameters and an int8 parameter-storage variant.

Figure 1 visualizes the 2-bit quality–size trade-off. Across both model families, HARP shifts the RHT curve downwards at nearly the same stored model size when int8 parameter storage is used. The improvement is greatest where the RHT model is farthest from FP16, while the gap naturally narrows for larger models whose 2-bit RHT baseline is already closer to full precision. This suggests HARP is most effective when fixed incoherence processing leaves substantial quantization error.

#### 4.1 Language modeling perplexity

Table 1 reports perplexity for QuIP# with fixed RHT and with HARP. Across the completed settings, replacing the fixed mixer with HARP consistently improves perplexity while keeping the quantizer backend, codebooks, random signs, and solver unchanged. The improvements are largest at 2 bits, where the quantizer is most sensitive to outliers and curvature anisotropy. A useful way to interpret the gains is as FP16-gap recovery: HARP reduces a

substantial fraction of the degradation introduced by the 2-bit RHT baseline, especially on the smaller and more quantization-sensitive models. Figure 1 visualizes this trend as a quality–size trade-off.

The 3- and 4-bit results show the expected pattern. As the bitrate increases, the fixed-RHT baseline is already closer to FP16, so the absolute room for improvement becomes smaller. Nevertheless, HARP continues to improve the perplexity, indicating that the benefit is not limited to a single extreme 2-bit setting. The relative benefit is strongest when the quantizer is most constrained, but the learned rotation remains useful at higher bitwidths.

Appendix B provides the full comparison to published AWQ, GPTQ, OmniQuant, and SpinQuant results at context length 2048.

#### Kronecker fallback and parameter storage.

The Kronecker fallback provides a lower-overhead 2-bit variant and closely matches QuIP#’s original non-power-of-two Hadamard convention, but it is generally less expressive than full Mixed-Radix HARP. Quantizing HARP parameters to int8 has little effect on perplexity in the completed experiments, suggesting that the learned processor can be stored compactly after fitting.

#### 4.2 Zero-shot evaluation

Table 2 reports zero-shot accuracy on Llama 2. At 2 bits, HARP improves most tasks over the fixed-RHT baseline, with the largest gains on ARC. On 13B, HARP improves ARC-Challenge, ARC-Easy, and WinoGrande, while PIQA remains close to the RHT baseline. These results indicate that the perplexity improvements are not only a likelihood artifact: the learned rotations also tend to improve downstream multiple-choice accuracy.

#### 4.3 Inference latency and storage

A central motivation for HARP is to improve incoherence processing without giving up the speed advantages of a quantized backend. We measure single-token latency using the QuIP# decoding-style microbenchmark: batch size 1, sequence length 1, one warmup pass, and 2000 timed repetitions, with CUDA graphs and SDPA attention enabled. CUDA graph capture avoids repeated small-kernel launch overhead. All timings in Table 3 use an NVIDIA RTX 5080 with 16GB VRAM.

HARP keeps most of the RHT throughput advantage while improving the quantized model quality. Across measured 2- and 4-bit settings, the added staged rotations introduce a modest latency

Table 1: Perplexity (PPL ↓) for QuIP# with fixed RHT and HARP. Llama 3.2 results use context length 8192; Llama 2 results use context length 4096. BPP counts base quantized weights plus processor overhead. HARP uses Mixed-Radix unless marked otherwise.

BITS	METHOD	LLAMA 3.2 1B			LLAMA 3.2 3B			LLAMA 2 7B			LLAMA 2 13B			LLAMA 2 70B		
		BPP	W2	C4	BPP	W2	C4	BPP	W2	C4	BPP	W2	C4	BPP	W2	C4
16	FP16	16.00	11.57	13.19	16.00	9.58	10.61	16.00	5.12	6.63	16.00	4.57	6.05	16.00	3.12	4.97
2	QuIP# (RHT)	2.00	26.27	25.24	2.00	16.59	15.88	2.00	8.22	10.86	2.00	6.05	8.06	2.00	4.16	6.01
2	HARP (KRONECKER)	2.13	23.36	22.88	2.06	15.97	15.29	2.02	7.61	9.98	—	—	—	—	—	—
2	+ INT8 PARAMS	2.07	23.38	22.90	2.03	16.06	15.30	2.01	7.67	10.06	—	—	—	—	—	—
2	HARP (MIXED-RADIX)	2.14	<b>22.30</b>	<b>22.57</b>	2.10	<b>15.02</b>	14.77	2.11	<b>7.23</b>	<b>9.49</b>	2.05	<b>5.71</b>	<b>7.63</b>	2.04	<b>4.01</b>	<b>5.81</b>
2	+ INT8 PARAMS	2.08	22.32	<b>22.57</b>	2.05	15.03	<b>14.76</b>	2.06	7.25	9.51	2.03	5.73	7.64	2.02	4.01	5.82
3	QuIP# (RHT)	3.00	14.02	15.32	3.00	11.04	11.72	3.00	5.61	7.35	3.00	4.89	6.49	3.00	3.40	5.20
3	HARP (MIXED-RADIX)	3.14	<b>13.46</b>	<b>14.56</b>	3.10	<b>10.60</b>	<b>11.50</b>	3.11	<b>5.51</b>	<b>7.19</b>	3.05	<b>4.81</b>	<b>6.38</b>	3.04	<b>3.35</b>	<b>5.15</b>
3	+ INT8 PARAMS	3.08	13.48	14.59	3.05	10.61	11.52	3.06	5.52	7.21	3.03	4.82	6.40	3.02	3.35	5.16
4	QuIP# (RHT)	4.00	12.37	13.95	4.00	10.13	11.04	4.00	5.27	6.85	4.00	4.70	6.20	4.00	3.22	5.05
4	HARP (MIXED-RADIX)	4.14	<b>12.17</b>	<b>13.66</b>	4.10	<b>9.88</b>	<b>10.80</b>	4.11	<b>5.22</b>	<b>6.78</b>	4.05	<b>4.64</b>	<b>6.14</b>	4.04	<b>3.19</b>	<b>5.02</b>
4	+ INT8 PARAMS	4.08	12.18	13.69	4.05	9.90	10.83	4.06	5.24	6.81	4.03	4.66	6.15	4.02	3.20	<b>5.02</b>

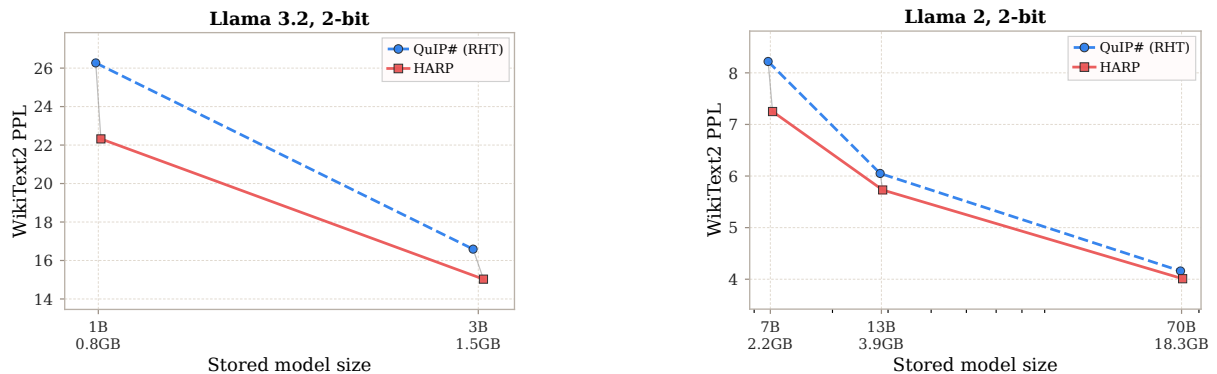


Figure 1: WikiText2 quality–size scaling at 2 bits. HARP uses int8 parameter storage. The plots are split by model family to keep the quality gaps visible across scales.

overhead relative to fixed RHT, but the 2-bit HARP model remains substantially faster than FP16 on 7B and enables 13B inference in a setting where FP16 does not fit. The overhead mainly comes from the extra stride-stage rotations. We use a fused Triton GPU kernel for each stride stage, avoiding materialized permutations and reducing HARP latency by approximately 20% relative to an unfused implementation. Calibration cost is reported separately in Appendix C, since it is a one-time model preparation cost. HARP’s storage overhead is also small after int8 parameter packing (see Appendix D).

#### 4.4 Backend portability: QTIP

As a portability check, we integrate the same HARP module into QTIP, which uses trellis-coded quantization together with incoherence processing (Tseng et al., 2024b). The integration only changes the preprocessing; and the QTIP backend remains fixed. Table 4 reports Llama 2 results at 2, 3 bits.

HARP improves QTIP across the completed settings, providing initial evidence that the processor is not specific to the QuIP# backend. The int8 variant preserves most gains. Because QTIP quantizes  $Q$ ,  $K$ , and  $V$  separately, their incoherence processors are also fit separately; sharing the input-side processor across these projections may be a natural way to reduce calibration cost in the future.

#### 4.5 Comparison with Published Baselines

Many published baselines report Llama 2 perplexity at context length 2048; Table 5 provides a context-matched comparison at this setting. At 2 bits, HARP outperforms QuIP# (RHT) by a large margin and surpasses all competitive scalar baselines, which largely fail at this aggressive compression level. Full results are provided in Appendix B.

### 5 Related Work

We organize related work into three parts: post-training quantization and its failure modes,

Table 2: Zero-shot accuracy (acc,  $\uparrow$ ) under QuIP# (RHT) vs. HARP on Llama 2 using 1m\_eval. HARP uses Mixed-Radix. Context length follows the evaluation harness defaults.

BITS	METHOD	LLAMA 2 7B					LLAMA 2 13B					LLAMA 2 70B				
		BPP	ARC	ARC	PIQA	WINO	BPP	ARC	ARC	PIQA	WINO	BPP	ARC	ARC	PIQA	WINO
16	FP16	16.00	40.0	69.3	78.5	67.3	16.00	45.6	73.3	73.5	69.6	16.00	51.1	77.7	81.1	77.0
2	QuIP# (RHT)	2.00	29.7	56.7	70.8	62.1	2.00	33.8	65.1	74.4	64.3	2.00	47.4	76.9	79.5	75.0
2	HARP	2.11	<b>33.0</b>	<b>63.7</b>	<b>72.4</b>	<b>62.9</b>	2.05	<b>36.4</b>	<b>67.3</b>	<b>75.8</b>	<b>67.2</b>	2.04	<b>48.5</b>	<b>77.8</b>	<b>79.9</b>	<b>75.5</b>
3	QuIP# (RHT)	3.00	37.7	<b>69.3</b>	76.2	66.7	3.00	41.4	71.6	77.5	68.0	3.00	50.4	78.4	<b>80.7</b>	<b>77.0</b>
3	HARP	3.11	<b>38.0</b>	69.1	<b>77.1</b>	<b>67.3</b>	3.05	<b>42.3</b>	<b>71.9</b>	<b>78.5</b>	<b>68.4</b>	3.04	<b>51.8</b>	<b>78.6</b>	80.6	76.8
4	QuIP# (RHT)	4.00	40.7	<b>70.6</b>	77.2	66.7	4.00	<b>45.6</b>	74.5	78.6	69.4	4.00	51.5	78.1	80.6	78.1
4	HARP	4.11	<b>40.7</b>	69.2	<b>78.3</b>	<b>68.7</b>	4.05	45.0	<b>74.8</b>	<b>78.9</b>	69.4	4.04	<b>51.9</b>	<b>78.2</b>	<b>81.2</b>	<b>78.4</b>

Table 3: Single-token latency on RTX 5080. HARP uses Mixed-Radix and int8 parameter storage.

MODEL	METHOD	BITS	SEC/TOKEN $\downarrow$	TOK/S $\uparrow$
LLAMA 2 7B	FP16	16	0.0162	61
	QuIP# (RHT)	2	0.0070	142
	HARP	2	0.0078	128
	QuIP# (RHT)	4	0.0100	100
	HARP	4	0.0110	91
LLAMA 2 13B	FP16	16	OOM	OOM
	QuIP# (RHT)	2	0.0110	91
	HARP	2	0.0119	84
	QuIP# (RHT)	4	0.0152	66
	HARP	4	0.0167	60

Table 4: Perplexity (PPL  $\downarrow$ ) for QTIP with fixed RHT and HARP. HARP uses Mixed-Radix.

BITS	METHOD	LLAMA 2 7B			LLAMA 2 13B	
		BPP	W2	C4	W2	C4
2	QTIP (RHT)	2.00	6.87	9.00	5.64	7.46
2	QTIP + HARP	2.10	<b>6.62</b>	<b>8.79</b>	<b>5.51</b>	<b>7.34</b>
2	+ INT8	2.05	6.63	8.91	5.52	7.36
3	QTIP (RHT)	3.00	5.41	7.03	4.75	6.31
3	QTIP + HARP	3.10	<b>5.37</b>	<b>6.98</b>	<b>4.74</b>	<b>6.26</b>
3	+ INT8	3.05	<b>5.37</b>	6.99	4.74	6.27

transform-based reparameterizations, and structured orthogonal transforms for quantization.

## 5.1 Post-Training Quantization of LLMs

### Heavy-Tailed Statistics and Outlier Channels.

Extreme low-bit quantization is dominated by heavy-tailed weight distributions and a small number of high-magnitude outlier channels that inflate per-tensor scales and reduce effective precision (Liu et al., 2024b; Ashkboos et al., 2024b). A direct remedy is to separate outliers and preserve them in higher precision: LLM.int8() (Dettmers et al., 2022) routes outlier features to fp16, while SpQR and SqueezeLLM decompose weights into a dense quantized core plus a sparse high-precision

Table 5: Context-matched 2-bit weight-only PTQ on Llama 2 at context length 2048. Baseline perplexities are taken from the respective papers.

Method	BPP	7B W2 $\downarrow$	7B C4 $\downarrow$	13B W2 $\downarrow$	13B C4 $\downarrow$
AWQ	2.14	$2.2 \times 10^5$	$1.7 \times 10^5$	$1.2 \times 10^5$	$9.4 \times 10^4$
GPTQ	2.14	36.77	33.70	28.14	20.97
OmniQuant	2.14	11.06	15.02	8.26	11.05
QuIP#	2.00	8.95	11.22	6.52	8.32
HARP	2.05	<b>7.85</b>	<b>9.68</b>	<b>6.13</b>	<b>7.87</b>

correction (Dettmers et al., 2023; Kim et al., 2023). QUIK extends the strategy to both weights and activations for end-to-end low-bit inference (Ashkboos et al., 2024a). Although effective, these methods introduce irregular memory access patterns and specialized kernel requirements that can negate the throughput advantages. This motivates approaches that maintain dense, uniform low-bit computation while reshaping layer statistics.

**Calibration-based rescaling.** A practical alternative to explicit outlier separation is to apply lightweight, calibration-guided channel-wise rescalings. AWQ derives per-channel scales from activation magnitudes to protect sensitive channels under weight-only quantization (Lin et al., 2024). SmoothQuant shifts part of the activation dynamic range into the weights via a matched diagonal rescaling, enabling standard integer kernels (Xiao et al., 2023). OmniQuant learns per-layer scale and clipping adjustments during calibration, though clipping is not a strict change of basis and can alter the function (Shao et al., 2023). While practical, diagonal rescaling cannot mix coordinates and therefore leaves correlated outlier subspaces intact – a limitation that grows increasingly severe at extreme bit widths. This motivates orthogonal reparameterizations that mix all coordinates while preserving the full-precision model exactly.

## 5.2 Transform-Based Reparameterizations

**Incoherence processing.** QuIP (Chee et al., 2023) introduces incoherence processing: it applies a structured random orthogonal change of basis so that weight mass and curvature-sensitive directions are spread across coordinates. QuIP# (Tseng et al., 2024a) replaces the general random orthogonals with the randomized Hadamard transform (RHT), which is exactly orthogonal and admits  $\mathcal{O}(d \log d)$  application. QTIP (Tseng et al., 2024b) retains the same preprocessing while advancing the quantizer backend to trellis-coded quantization. Beyond weight-only PTQ, QuaRot (Ashkboos et al., 2024b) inserts discrete orthogonal rotations into the full Transformer graph to suppress outliers in weights, activations, and the KV cache. A shared limitation of all these methods is the fixed transform.

**Learned model-level rotations.** SpinQuant (Liu et al., 2024b) demonstrates that the choice of rotation substantially affects low-bit quality and learns Transformer-invariant rotations (including residual-stream and attention-head rotations) end-to-end against a quantized-network objective. The learned rotations are *model-level* objects wired into the Transformer graph, making SpinQuant an important baseline but not a drop-in replacement for the two-sided Hadamard preprocessor inside QuIP#-style pipelines. HARP, in contrast, operates at the level of a single linear layer and is fit within the PTQ calibration loop – it is designed as a reusable processor module for backends that already expose an incoherence-processing step.

**Non-orthogonal data-aware transforms.** WUSH (Chen et al., 2025) derives closed-form near-optimal blockwise transforms for joint weight–activation quantization under RTN AbsMax-scaled quantizers, combining a Hadamard backbone with a calibration-dependent second-moment factor. The resulting transform is generally non-orthogonal and targets standard RTN-style block quantizers at 4-bit weight/activation precision – a different operating point from HARP’s focus on extreme low-bit PTQ (2–3 bits per weight) with vector-quantized backends. More fundamentally, non-orthogonal transforms alter the full-precision computation and are not drop-in change-of-basis modules; HARP deliberately stays strictly orthogonal so the full-precision model is preserved exactly.

**Rate allocation, information-theoretic views.** WaterSIC (Lifar et al., 2026) analyzes linear-layer quantization through rate–distortion theory and derives a waterfilling allocation across input columns. Q-Palette (Lee and Song, 2026) connects near-optimal Gaussian-weight bit allocation with practical fractional-bit quantizers. Both are complementary to HARP: they modify bit allocation or the quantizer family, whereas HARP modifies the orthogonal basis for a fixed backend.

**Structured code families.** The effectiveness of extreme low-bit PTQ depends heavily on the quantizer code family. AQLM (Egiazarian et al., 2024) achieves extreme compression through additive multi-codebook quantization. GPTVQ and VPTQ demonstrate that Hessian-aware vector quantization can improve the size–accuracy trade-off by quantizing higher-dimensional weight blocks (Van Baalen et al., 2024; Liu et al., 2024a). QuIP# combines incoherence processing with lattice/codebook vector quantization, while QTIP replaces explicit codebooks with trellis coding to increase the effective quantization dimension (Tseng et al., 2024a,b). As these backends grow more powerful, the choice of coordinate system becomes more consequential: HARP learns this coordinate system, leaving the chosen backend unchanged.

## 5.3 Structured Orthogonal Transforms

The closest direction to HARP is the use of learnable structured orthogonal rotations as quantization preprocessors. ButterflyQuant (Xu et al., 2025) replaces fixed Hadamard rotations with learnable butterfly transforms parameterized by continuous Givens rotations, preserving orthogonality and  $\mathcal{O}(d \log d)$  cost while adapting the rotation to calibration data. HARP shares the principle that structured orthogonal transforms provide learnable mixing at deployable cost, but differs in target and compatibility constraints.

Specifically, HARP is designed as a drop-in replacement for the two-sided RHT inside QuIP#-style PTQ pipelines, with four distinguishing properties. First, HARP initializes exactly to the corresponding RHT preprocessor (up to a fixed permutation convention), so calibration learns a structured refinement around an already-strong baseline rather than from scratch. Second, HARP uses Hadamard-preconditioned block kernels and supports non-power-of-two dimensions through Mixed-Radix schedules without padding. Third, HARP optimizes a layerwise objective directly

coupled to the deployed blockwise quantizer, including a block-diagonalization regularizer that aligns the learned curvature with the backend’s block structure. Fourth, HARP is compatible with modern vector-quantized backends such as QuIP# and QTIP, enabling backend-agnostic deployment.

**Summary of positioning.** Relative to fixed RHT (Tseng et al., 2024a,b), HARP preserves fast structured execution while adding per-layer, backend-aware adaptivity. Relative to model-level learned rotations (Liu et al., 2024b), HARP uses a staged structured parameterization with controlled overhead and does not require rewiring the Transformer graph. Relative to non-orthogonal data-aware transforms (Chen et al., 2025), HARP stays strictly orthogonal so the full-precision model is preserved exactly. Rather than proposing a new standalone pipeline or quantizer, HARP treats the incoherence processor as a reusable module insertable into any Hadamard-based backbone.

## 6 Conclusion

We introduced HARP, a learnable structured orthogonal incoherence processor for low-bit PTQ. HARP initializes exactly to the fixed RHT and learns a layer- and backend-aware refinement from calibration data. Using Mixed-Radix butterfly-like stages, HARP supports practical transformer dimensions at controlled overhead and can be stored compactly in int8. Across Llama 3.2 and Llama 2 at 2–4 bits, HARP consistently improves over fixed RHT under the QuIP# backend – with the largest gains at 2 bits – and transfers to QTIP with no backend changes. The processor can be stored compactly with int8 parameters, and latency measurements show that HARP preserves most of the throughput advantage of the quantized model.

## Limitations

HARP adds a one-time calibration cost that is larger than applying a fixed RHT. Refreshing the quantized target less frequently reduces this overhead (Appendix C), but improving calibration efficiency remains an open direction.

HARP is evaluated for weight-only PTQ, matching the focus of the baselines we compare against (QuIP#, AWQ, GPTQ). A comparison against rotations under a weight–activation backend requires inserting activation rotations into the model graph and handling interactions with KV-cache quantization, attention kernels, and residual-stream invariance, and remains future work.

## Acknowledgments

We thank Ekaterina Alimaskina for her assistance with discussions and the experimental setup.

## References

- Saleh Ashkboos, Iliia Markov, Elias Frantar, Tingxuan Zhong, Xincheng Wang, Jie Ren, Torsten Hoefer, and Dan Alistarh. 2024a. Quik: Towards end-to-end 4-bit inference on generative large language models. In *Proceedings of the 2024 Conference on Empirical Methods in Natural Language Processing*, pages 3355–3371.
- Saleh Ashkboos, Amirkeivan Mohtashami, Maximilian L Croci, Bo Li, Pashmina Cameron, Martin Jaggi, Dan Alistarh, Torsten Hoefer, and James Hensman. 2024b. Quarot: Outlier-free 4-bit inference in rotated llms. *Advances in Neural Information Processing Systems*, 37:100213–100240.
- Jerry Chee, Yaohui Cai, Volodymyr Kuleshov, and Christopher M De Sa. 2023. Quip: 2-bit quantization of large language models with guarantees. *Advances in Neural Information Processing Systems*, 36:4396–4429.
- Jiale Chen, Vage Egiazarian, Torsten Hoefer, and Dan Alistarh. 2025. Wush: Near-optimal adaptive transforms for llm quantization. *arXiv preprint arXiv:2512.00956*.
- Tim Dettmers, Mike Lewis, Younes Belkada, and Luke Zettlemoyer. 2022. Gpt3. int8 (): 8-bit matrix multiplication for transformers at scale. *Advances in neural information processing systems*, 35:30318–30332.
- Tim Dettmers, Ruslan Svirschevski, Vage Egiazarian, Denis Kuznedelev, Elias Frantar, Saleh Ashkboos, Alexander Borzunov, Torsten Hoefer, and Dan Alistarh. 2023. Spqr: A sparse-quantized representation for near-lossless llm weight compression. *arXiv preprint arXiv:2306.03078*.
- Vage Egiazarian, Andrei Panferov, Denis Kuznedelev, Elias Frantar, Artem Babenko, and Dan Alistarh. 2024. Extreme compression of large language models via additive quantization. *arXiv preprint arXiv:2401.06118*.
- Elias Frantar and Dan Alistarh. 2022. Optimal brain compression: A framework for accurate post-training quantization and pruning. *Advances in Neural Information Processing Systems*, 35:4475–4488.
- Elias Frantar, Saleh Ashkboos, Torsten Hoefer, and Dan Alistarh. 2022. Gptq: Accurate post-training quantization for generative pre-trained transformers. *arXiv preprint arXiv:2210.17323*.
- Babak Hassibi and David Stork. 1992. Second order derivatives for network pruning: Optimal brain surgeon. *Advances in neural information processing systems*, 5.

Babak Hassibi, David Stork, and Gregory Wolff. 1993. Optimal brain surgeon: Extensions and performance comparisons. *Advances in neural information processing systems*, 6.

Sehoon Kim, Coleman Hooper, Amir Gholami, Zhen Dong, Xiuyu Li, Sheng Shen, Michael W Mahoney, and Kurt Keutzer. 2023. Squeezellm: Dense-and-sparse quantization. *arXiv preprint arXiv:2306.07629*.

Deokjae Lee and Hyun Oh Song. 2026. Q-palette: Fractional-bit quantizers toward optimal bit allocation for efficient llm deployment. *Advances in Neural Information Processing Systems*, 38:11525–11558.

Egor Lifar, Semyon Savkin, Or Ordentlich, and Yury Polyanskiy. 2026. Watersic: information-theoretically (near) optimal linear layer quantization. *arXiv preprint arXiv:2603.04956*.

Ji Lin, Jiaming Tang, Haotian Tang, Shang Yang, Weiming Chen, Wei-Chen Wang, Guangxuan Xiao, Xingyu Dang, Chuang Gan, and Song Han. 2024. Awq: Activation-aware weight quantization for on-device llm compression and acceleration. *Proceedings of machine learning and systems*, 6:87–100.

Yifei Liu, Jicheng Wen, Yang Wang, Shengyu Ye, Li Lina Zhang, Ting Cao, Cheng Li, and Mao Yang. 2024a. Vptq: Extreme low-bit vector post-training quantization for large language models. In *Proceedings of the 2024 Conference on Empirical Methods in Natural Language Processing*, pages 8181–8196.

Zechun Liu, Changsheng Zhao, Igor Fedorov, Bilge Soran, Dhruv Choudhary, Raghuraman Krishnamoorthi, Vikas Chandra, Yuandong Tian, and Tijmen Blankevoort. 2024b. Spinquant: Llm quantization with learned rotations. *arXiv preprint arXiv:2405.16406*.

Wenqi Shao, Mengzhao Chen, Zhaoyang Zhang, Peng Xu, Lirui Zhao, Zhiqian Li, Kaipeng Zhang, Peng Gao, Yu Qiao, and Ping Luo. 2023. Omniquant: Omnidirectionally calibrated quantization for large language models. *arXiv preprint arXiv:2308.13137*.

Albert Tseng, Jerry Chee, Qingyao Sun, Volodymyr Kuleshov, and Christopher De Sa. 2024a. Quip#: Even better llm quantization with hadamard incoherence and lattice codebooks. *arXiv preprint arXiv:2402.04396*.

Albert Tseng, Qingyao Sun, David Hou, and Christopher M De Sa. 2024b. Qtip: Quantization with trellises and incoherence processing. *Advances in Neural Information Processing Systems*, 37:59597–59620.

Mart Van Baalen, Andrey Kuzmin, Ivan Koryakovskiy, Markus Nagel, Peter Couperus, Cedric Bastoul, Eric Mahurin, Tijmen Blankevoort, and Paul Whatmough. 2024. Gptvq: The blessing of dimensionality for llm quantization. *arXiv preprint arXiv:2402.15319*.

Diyuan Wu, Ionut-Vlad Modoranu, Mher Safaryan, Denis Kuznedelev, and Dan Alistarh. 2024. The iterative optimal brain surgeon: Faster sparse recovery by leveraging second-order information. *Advances in Neural Information Processing Systems*, 37:139621–139649.

Guangxuan Xiao, Ji Lin, Mickael Seznec, Hao Wu, Julien Demouth, and Song Han. 2023. Smoothquant: Accurate and efficient post-training quantization for large language models. In *International conference on machine learning*, pages 38087–38099. PMLR.

Bingxin Xu, Zhen Dong, Oussama Elachqar, and Yuzhang Shang. 2025. Butterflyquant: Ultra-low-bit llm quantization through learnable orthogonal butterfly transforms. *arXiv preprint arXiv:2509.09679*.

## A Hadamard stride factorization and initialized equivalence

**Goal.** We prove that HARP at  $\Theta = 0$  recovers Hadamard-family incoherence processing under the conventions used in the main text. We show: (i) the Walsh–Hadamard transform admits a stride-stage factorization, (ii) initialized HARP implements this factorization up to a fixed permutation, and (iii) the Kronecker fallback matches the corresponding QuIP# convention.

**Conventions.** We work with column vectors in this appendix for clarity. The row-vector convention used in the main text is the transpose of these statements. For  $b = 2^k$ , let the unnormalized Sylvester matrices be defined by

$$\tilde{H}_1 = [1], \quad \tilde{H}_{2n} = \begin{bmatrix} \tilde{H}_n & \tilde{H}_n \\ \tilde{H}_n & -\tilde{H}_n \end{bmatrix},$$

and define  $H_b := b^{-1/2} \tilde{H}_b$ . Then  $H_b^\top H_b = I_b$ .

### A.1 Walsh–Hadamard as stride stages

Assume  $d = b^m$  with  $b = 2^k$ . For stage  $t \in \{0, \dots, m-1\}$ , define

$$s_t := b^t, \quad g_t := \frac{d}{b s_t} = b^{m-t-1},$$

and the stride stage

$$S_t := I_{g_t} \otimes H_b \otimes I_{s_t}.$$

**Lemma 2** (Stride implementation equals the Kronecker stage). *Let  $x \in \mathbb{R}^d$ . Reshape  $x$  into  $X \in \mathbb{R}^{g_t \times b \times s_t}$  by*

$$X[\alpha, r, \beta] := x[\alpha(b s_t) + r s_t + \beta].$$

*Apply  $H_b$  along the middle index  $r$  independently for each  $(\alpha, \beta)$ , and flatten back using the same indexing convention. The resulting vector is  $S_t x$ .*

*Proof.* For fixed  $(\alpha, \beta)$ , the operation multiplies the length- $b$  vector over index  $r$  by  $H_b$  and leaves

all other indices unchanged. This is exactly the action of  $I_{g_t} \otimes H_b \otimes I_{s_t}$  under the stated flattening order.  $\square$

Define

$$\mathcal{H}_d^{\text{stride}} := S_{m-1} \cdots S_0.$$

**Lemma 3** (Stride product is a Hadamard transform up to permutation). *There exists a fixed permutation matrix  $P$  depending only on the digit/reshape convention such that*

$$\mathcal{H}_d^{\text{stride}} = P^\top H_d P.$$

*Proof.* Write each index as base- $b$  digits,  $i = \sum_{\ell=0}^{m-1} i_\ell b^\ell$ . Stage  $S_t$  mixes digit  $i_t$  and holds all other digits fixed. The product therefore applies  $H_b$  once per digit, i.e., it is  $H_b^{\otimes m}$  up to a digit-axis permutation. That permutation is represented by  $P$ . Under the Sylvester convention,  $H_d = H_b^{\otimes m}$ .  $\square$

## A.2 Initialized HARP equals the stride Hadamard mixer

**Theorem 4** (Exact equivalence at  $\Theta = 0$ ). *Assume  $d = b^m$  with  $b = 2^k$ , and HARP uses  $G_b = H_b$  for every stage. At initialization,  $Q_{t,c}(0) = I$  for all stages and blocks. Then*

$$T(0) = \mathcal{H}_d^{\text{stride}} = P^\top H_d P.$$

*Proof.* At initialization, every HARP block is  $B_{t,c}(0) = Q_{t,c}(0)G_b = H_b$ . Thus each HARP stage is exactly the stride stage  $S_t$  from Lemma 2. Taking the product over stages gives  $T(0) = S_{m-1} \cdots S_0 = \mathcal{H}_d^{\text{stride}}$ . The final equality follows from Lemma 3.  $\square$

## A.3 Kronecker fallback

Assume  $d = K \cdot 2^L$  and  $\tilde{H}_K \in \{\pm 1\}^{K \times K}$  satisfies  $\tilde{H}_K \tilde{H}_K^\top = K I_K$ . Let  $H_K := \tilde{H}_K / \sqrt{K}$ . The Kronecker fallback defines

$$T_d(\Theta) = H_K \otimes T_{2L}(\Theta).$$

**Corollary 5** (Exact Kronecker equivalence at  $\Theta = 0$ ). *If  $T_{2L}(0) = P^\top H_{2L} P$ , then*

$$T_d(0) = (I_K \otimes P)^\top (H_K \otimes H_{2L}) (I_K \otimes P).$$

*Thus the initialization matches the Kronecker–Hadamard preprocessing convention up to the same fixed permutation on the power-of-two axis.*

*Proof.* Substitute  $T_{2L}(0) = P^\top H_{2L} P$  and use the mixed-product property of Kronecker products.  $\square$

## B Comparison to published PTQ baselines

The main Llama 2 results in Table 1 use context length 4096. Many published AWQ, GPTQ, and OmniQuant weight-only results instead report Llama 2 perplexity at context length 2048. Table 6 therefore reports a separate context-matched comparison. For AWQ, GPTQ, OmniQuant, and SpinQuant, we use the values reported in the corresponding papers; for fixed-RHT QuIP# and HARP, we reevaluate using context length 2048. Because grouped scalar baselines use method-specific metadata and scale storage conventions, BPP values should be read as approximate effective bitrates.

At 2 and 3 bits, HARP outperforms the strongest published scalar baselines in this context-matched comparison. At 4 bits, the gap is small because all competitive methods are close to FP16; HARP remains comparable and slightly improves C4. These results are system-level comparisons because the baselines use different quantizers and calibration procedures. The isolated processor comparison remains fixed RHT versus HARP under the same QuIP# backend.

## C Calibration-time cost

HARP adds a one-time layerwise fitting stage before quantization. The dominant cost is recomputing the stopped-gradient quantized target  $Q(\tilde{W})$  during optimization. To test whether this target must be refreshed every step, we run a target-refresh ablation on Llama 2 7B at 2 bits. All runs use 1200 HARP optimizer steps per layer block and context length 4096 for evaluation.

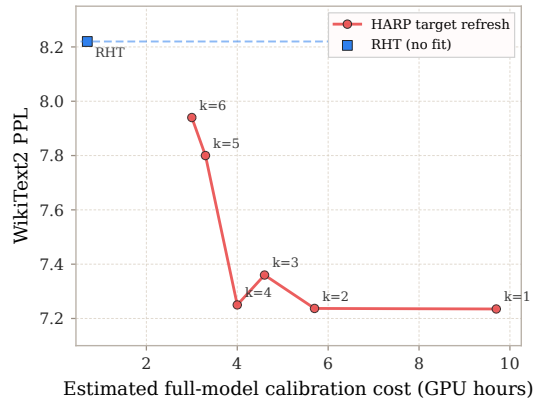


Figure 2: Calibration cost–quality trade-off for the target-refresh ablation in Table 7.

Refreshing every two steps reduces the estimated

Table 6: Context-matched weight-only PTQ comparison on Llama 2 at context length 2048. HARP denotes the QuIP# backend with its fixed RHT mixer replaced by HARP.

Bits	Method	Eff. BPP	7B W2	7B C4	13B W2	13B C4
2	AWQ (g128)	2.14	$2.2 \times 10^5$	$1.7 \times 10^5$	$1.2 \times 10^5$	$9.4 \times 10^4$
2	GPTQ (g128)	2.14	36.77	33.70	28.14	20.97
2	OmniQuant (g128)	2.14	11.06	15.02	8.26	11.05
2	QuIP# (RHT)	2.00 / 2.00	8.95	11.22	6.52	8.32
2	HARP	2.11 / 2.05	<b>7.85</b>	<b>9.68</b>	<b>6.13</b>	<b>7.87</b>
3	AWQ (g128)	3.15	6.24	7.84	5.32	6.94
3	GPTQ (g128)	3.15	6.29	7.89	5.42	7.00
3	OmniQuant (g128)	3.15	6.03	7.75	5.28	6.98
3	QuIP# (RHT)	3.00 / 3.00	6.00	7.60	5.23	6.85
3	HARP	3.11 / 3.05	<b>5.89</b>	<b>7.46</b>	<b>5.15</b>	<b>6.74</b>
4	AWQ (g128)	4.16	5.62	7.13	4.97	6.56
4	GPTQ (g128)	4.16	5.61	7.12	4.98	6.56
4	OmniQuant (g128)	4.16	<b>5.58</b>	7.12	<b>4.95</b>	6.56
4	SpinQuant	—	5.6	—	5.0	—
4	QuIP# (RHT)	4.00 / 4.00	5.64	7.16	5.01	6.60
4	HARP	4.11 / 4.05	5.59	<b>7.10</b>	4.96	<b>6.55</b>

Table 7: Calibration-time ablation on Llama 2 7B, 2-bit HARP. The refresh interval  $k$  means that  $Q(\tilde{W})$  is recomputed once every  $k$  optimizer steps.

METHOD / $k$	LAYER-BLOCK TIME	EST. FULL-MODEL TIME	W2 PPL ↓
RHT	~ 80s	~ 0.7H	8.22
HARP, $k = 1$	~ 1100s	~ 9.7H	7.235
HARP, $k = 2$	~ 650s	~ 5.7H	7.237
HARP, $k = 3$	~ 520s	~ 4.6H	7.36
HARP, $k = 4$	~ 450s	~ 4.0H	7.25
HARP, $k = 5$	~ 370s	~ 3.3H	7.80
HARP, $k = 6$	~ 340s	~ 3.0H	7.94

full-model fitting time from about 9.7 to 5.7 GPU-hours with essentially unchanged WikiText2 perplexity. Refreshing every four steps reduces the estimate further to about 4.0 GPU-hours while preserving most of the quality gain over RHT. Larger refresh intervals begin to degrade quality more noticeably. These results indicate that HARP’s calibration cost can be reduced without changing the inference-time model, but calibration efficiency remains an important limitation.

## D Stored model size

Table 8 reports stored model size in GB for the fixed-RHT baseline, HARP with floating-point parameters, and HARP with int8 parameter storage. All sizes include the quantized model and processor metadata.

Table 8: Stored model size in GB.

Bits	MODEL	RHT	HARP	HARP-INT8
2	LLAMA 3.2 1B	0.77	0.82	0.78
2	LLAMA 3.2 3B	1.50	1.60	1.52
2	LLAMA 2 7B	2.15	2.41	2.20
2	LLAMA 2 13B	3.84	4.12	3.89
2	LLAMA 2 70B	18.18	19.21	18.38
3	LLAMA 3.2 1B	0.90	0.95	0.91
3	LLAMA 3.2 3B	1.85	1.96	1.87
3	LLAMA 2 7B	2.96	3.22	3.01
3	LLAMA 2 13B	5.43	5.70	5.48
3	LLAMA 2 70B	26.75	27.78	26.95
4	LLAMA 3.2 1B	1.02	1.07	1.03
4	LLAMA 3.2 3B	2.21	2.31	2.23
4	LLAMA 2 7B	3.77	4.03	3.82
4	LLAMA 2 13B	7.01	7.29	7.07
4	LLAMA 2 70B	35.32	36.35	35.52

## E Incoherence and quantizer-alignment diagnostics

The purpose of incoherence processing is to change the coordinate system in which the quantizer operates, not to change the full-precision function. A fixed RHT spreads energy generically, while HARP learns a structured orthogonal refinement that is optimized for the layer and backend. To test this mechanism, we compute layerwise diagnostics on Llama 2 7B under 2-bit QuIP# quantization and report means over evaluated linear modules.

We measure five quantities.  $\mu_W(\tilde{W}_{pre})$  is QuIP’s weight incoherence score on the rotated dense weight before quantization.  $\mu_W(\tilde{W})$  is the same score after quantization in the processed basis.

OffBlk( $\tilde{H}$ ) is the fraction of rotated Hessian energy lying outside the contiguous block structure used by the quantizer; lower values mean that the blockwise backend better matches the second-order geometry.  $\mathcal{L}_{\text{diag}}(\tilde{W})$  is the diagonal Hessian-weighted distortion used by the HARP fitting proxy. Finally,  $\mu_H(\tilde{H})$  is the classical QuIP Hessian incoherence score. Lower is better for all metrics.

Table 9: Incoherence and quantizer-alignment diagnostics on Llama 2 7B, 2-bit HARP. ‘‘HARP better’’ counts the number of evaluated modules where HARP improves over RHT.

METRIC	RHT	HARP	$\Delta$	HARP BETTER
$\mu_W(\tilde{W}_{\text{pre}})$	5.7712	<b>5.0972</b>	-0.6741	118 / 128
$\mu_W(\tilde{W})$	3.0159	<b>3.0049</b>	-0.0110	125 / 128
OffBlk( $\tilde{H}$ )	0.9634	<b>0.9237</b>	-0.0397	103 / 128
$\mathcal{L}_{\text{diag}}(\tilde{W})$	$2.538 \times 10^{-4}$	<b><math>2.493 \times 10^{-4}</math></b>	$-4.57 \times 10^{-6}$	126 / 128
$\mu_H(\tilde{H})$	<b>6.5997</b>	11.2700	+4.6703	13 / 96

The diagnostics support the intended mechanism with an important nuance. HARP improves pre-quantization weight incoherence, quantized-weight incoherence, off-block Hessian energy, and the diagonal Hessian-weighted distortion in almost all evaluated modules. However, it does not improve the classical Hessian incoherence score  $\mu_H$ ; in fact, RHT is better on this generic metric. This is consistent with HARP’s objective. HARP is not trained to make the layer maximally incoherent under every definition. It is trained to find an exact orthogonal basis that is more favorable for the deployed blockwise quantizer. The quality gains in Table 1 therefore appear to come from quantizer-aligned rotation learning rather than from uniformly improving all classical incoherence scores.

## F Additional experiments

### F.1 Ablation: stage radix as a quality/overhead knob

The stage radix controls both expressivity and overhead. For fixed dimension  $d$ , larger radix reduces the number of stride stages (e.g., for  $d = 4096$ , the stage count is  $\log_b d$ ), which can reduce reshape/transpose and kernel-launch overhead in practice. However, larger blocks have more degrees of freedom and therefore increase parameter overhead, which is reflected in BPP. Table 10 shows this trade-off on Llama 2 7B.

Table 10: Effect of the preferred radix  $b$  on Llama 2 7B (2-bit PTQ)

$b$	STAGES (4096)	BPP	W2 PPL ↓	C4 PPL ↓
2	12	2.08	7.38	9.73
4	6	2.09	7.36	9.65
8	4	2.11	7.23	9.49
16	3	2.15	<b>7.17</b>	<b>9.35</b>

Table 11: Base mixer choice for HARP blocks on Llama 2 7B, 2-bit PTQ.

MIXER	W2 PPL ↓	C4 PPL ↓
IDENTITY ( $G_b = I$ )	7.29	9.61
HADAMARD+QR	<b>7.23</b>	<b>9.49</b>

### F.2 Ablation: base mixer choice

Table 11 compares using an identity base mixer against the default Hadamard/QR base mixers. Hadamard preconditioning provides a stronger initialization and slightly improves the final perplexity.

## G Additional scaling plots

Figure 3 shows WikiText2 quality–size scaling at 3 and 4 bits. The absolute gains are smaller than at 2 bits because the RHT baseline is already closer to FP16, but HARP continues to shift the curve downward at nearly unchanged storage when int8 parameter storage is used.

## H Compatibility with QuIP# fine-tuning

The main experiments compare no-finetuning quantization to isolate the effect of the incoherence processor. QuIP# also reports results with additional fine-tuning stages. We distinguish two such stages.

*FT-quant* denotes QuIP#’s fine-tuning-during-quantization stage. Modules within each Transformer block are quantized in a fixed order, starting with the joint  $QKV$  projection. After the current module or module group is quantized, optimization updates the channel scales for modules that have already been quantized and the full weights for modules that have not yet been quantized. Thus, FT-quant locally adapts the partially quantized block while quantization proceeds through the block.

*E2E FT* denotes the subsequent end-to-end fine-tuning stage after all modules have been quantized. At this stage, the procedure fine-tunes quantization scales together with the remaining unquantized parameters in the network, such as normalization parameters and the language-model head.

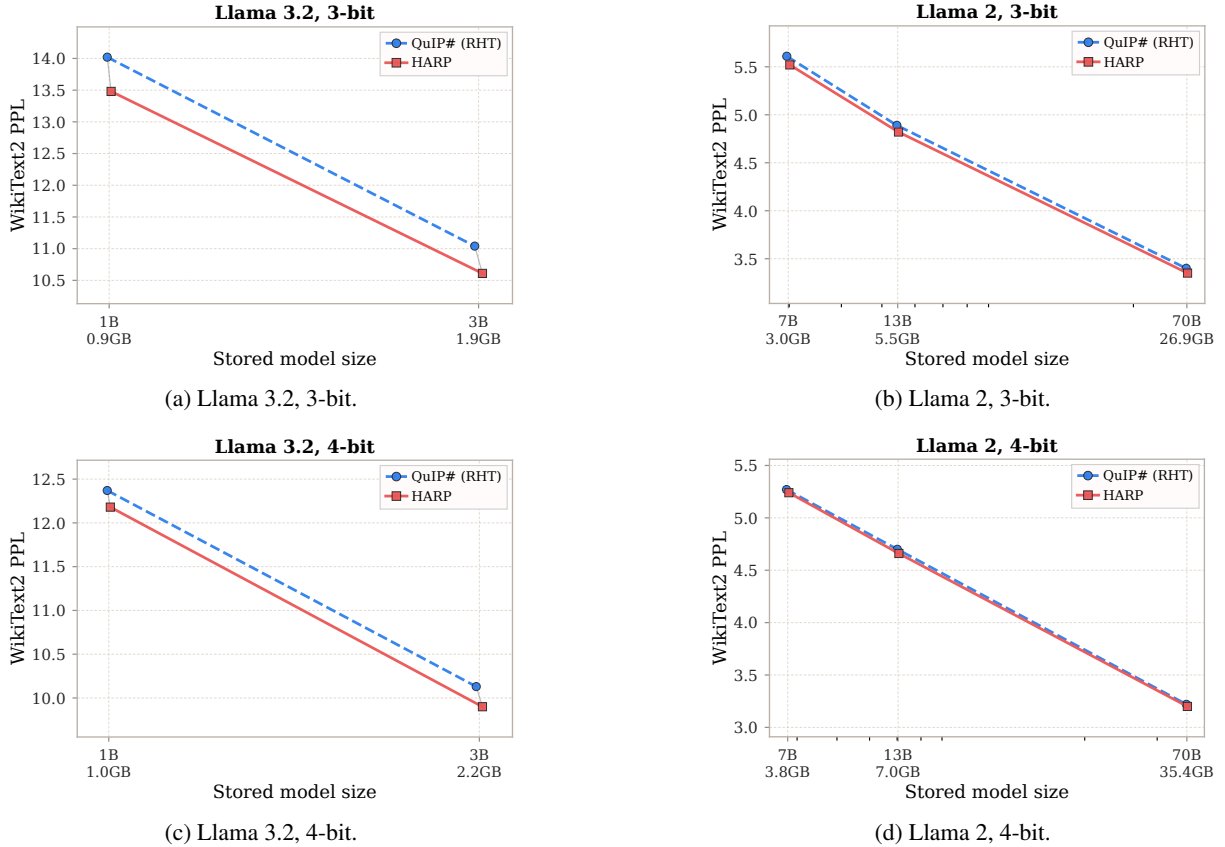


Figure 3: WikiText2 quality–size scaling at 3 and 4 bits. HARP uses int8 parameter storage. Llama 3.2 models use context length 8192; Llama 2 models use context length 4096.

These stages improve final quality, but they introduce additional choices such as trainable parameter sets, learning rates, schedules, and data budgets. For this reason, our main tables omit them and isolate the RHT-to-HARP processor change.

HARP is compatible with these stages because it only changes the orthogonal preprocessing used before quantization. As a preliminary check, we enable FT-quant on Llama 2 7B at context length 4096. Table 12 reports the result.

Table 12: Fine-tuning compatibility on Llama 2 7B, 2-bit, context length 4096. HARP uses Mixed-Radix.

METHOD	W2 PPL ↓	C4 PPL ↓
QUIP# + RHT + FT-QUANT ONLY	6.44	8.30
QUIP# + RHT + FT-QUANT + E2E FT	6.19	8.16
HARP + FT-QUANT ONLY	<b>6.16</b>	<b>8.08</b>

Even with only FT-quant, HARP improves over the corresponding RHT setting. It also slightly improves over the fully tuned RHT result that uses both FT-quant and E2E FT. We do not include full HARP + E2E FT experiments in the main table because the goal is to isolate the processor and avoid conflating it with fine-tuning schedule choices.

## I Experimental Reproducibility Checklist

### I.1 Hardware

Quantization and calibration experiments were run on NVIDIA H100 GPUs unless otherwise stated. Inference latency in Section 4.3 was measured on an NVIDIA GeForce RTX 5080 with 16GB VRAM. For Llama 2 7B at 2 bits with 1200 HARP steps per layer block, refreshing the quantized target every optimizer step gives an estimated full-model fitting time of about 9.7 GPU-hours in our setup, excluding Hessian generation. Refreshing the target every four steps reduces this estimate to about 4.0 GPU-hours with a small quality change (Appendix C). Hessian generation is a separate one-time preprocessing step and can be reused across methods and hyperparameter sweeps.

### I.2 Evaluation

Unless otherwise stated, reported perplexity and zero-shot entries are from a single quantization/evaluation run under the specified recipe; layerwise diagnostics report means over evaluated modules.

### I.3 HARP fitting hyperparameters

Unless stated otherwise, we fit one pair of HARP processors ( $U, V$ ) per linear layer using  $S = 1200$  Adam steps. We use stride ordering (Algorithm 1) with a single pass ( $P = 1$ ) and the default Mixed-Radix schedule constructed by Algorithm 2 with preferred radix  $b_{\text{base}} = 8$  and maximum radix  $b_{\text{max}} = 8$ .

**QuIP# hyperparameters.** We keep the QuIP# backend fixed throughout: codebook family and training, block sizes, quantization scales, and all QuIP# solver/rounding hyperparameters follow the settings in the original QuIP# paper (Tseng et al., 2024a). We do not retune QuIP#-specific hyperparameters for HARP; the only change is replacing the fixed Hadamard mixer with the learned HARP processor (and optionally enabling the Kronecker fallback where stated).

**Calibration statistics.** For HARP fitting we reuse the precomputed Hessian/second-moment statistics from the corresponding QuIP# pipeline when available. Following the QuIP# protocol, these statistics are computed from 6144 sequences sampled from RedPajama 1T at the model’s native context length (Tseng et al., 2024a). Hessian generation is a one-time preprocessing step and can be reused across quantization methods, hyperparameter sweeps, and HARP target-refresh settings.

**Optimization.** We use learning rates  $\eta_U = \eta_V = 3 \times 10^{-2}$  for the  $U$  and  $V$  parameters. We initialize rotation parameters at  $\Theta = 0$ , so that  $Q_{t,c}(0) = I$  and HARP matches Hadamard-family preprocessing at initialization (Section 3.2).

**Objective and regularization.** We use the diagonal-weighted proxy objective from Eq. (14) and the block-diagonalization regularizer from Eq. (15) with  $\lambda_{\text{bd}} = 0.1$  and block size  $g = 8$ .

**Base mixers.** For power-of-two radices we use Hadamard base mixers, and for non-power-of-two radices we use the QR-based orthogonal fallback (Section 3.1).

### I.4 Artifacts and licenses

We use publicly released Llama 2 and Llama 3.2 checkpoints under their original model licenses, and evaluate on WikiText2, C4, ARC-Challenge, ARC-Easy, PIQA, and WinoGrande through the standard evaluation harness. We release anonymized software for reproducing HARP experiments and plan to release quantized HARP checkpoints for research and reproducibility. The

quantized checkpoints are derived from the corresponding base models and remain subject to the original model licenses and access terms. We do not redistribute benchmark data or calibration text. The released software is an anonymized fork of public QuIP# and QTIP implementations with HARP additions and follows the upstream licenses stated in the repository README.

## J Implementation details

This section reports implementation details omitted from the main text: the stride-layout example, the Mixed-Radix schedule construction, the layer-wise fitting pseudocode, and parameter packing.

### J.1 Stride-stage implementation

The permutation  $P_t$  in Eq. (7) is conceptual. A stage is implemented by reshaping, transposing, multiplying small blocks, and reshaping back.

**Index-view example.** For  $d = 16$  and  $b = 4$ , write an index as two base-4 digits  $i = i_0 + 4i_1$ . The first stage mixes the low-order digit  $i_0$  while holding  $i_1$  fixed; these are contiguous groups. The second stage mixes the high-order digit  $i_1$  while holding  $i_0$  fixed; these are stride-4 groups. Thus each stage mixes one digit of the Mixed-Radix index representation, as in fast Walsh–Hadamard and Cooley–Tukey-style transforms, but implemented by reshape/transpose rather than by materializing a permutation.

### J.2 Stage schedules and Mixed-Radix construction

---

**Algorithm 2** Greedy Mixed-Radix schedule (preferred radix first)

---

**Require:** Dimension  $d \geq 2$ , preferred radix  $b_{\text{base}}$  (default 8), maximum radix  $b_{\text{max}}$  (default 8)

**Ensure:** A list of stage radices  $\mathbf{b} = (b_0, \dots, b_{m-1})$  such that

```
 $\prod_t b_t = d$   
1:  $\mathbf{b} \leftarrow []$ ,  $r \leftarrow d$   
2: while  $r \bmod b_{\text{base}} = 0$  do  
3:   append  $b_{\text{base}}$  to  $\mathbf{b}$   
4:    $r \leftarrow r/b_{\text{base}}$   
5: end while  
6: for  $f = \min(b_{\text{max}}, r)$  down to 2 do  
7:   while  $r \bmod f = 0$  do  
8:     append  $f$  to  $\mathbf{b}$   
9:      $r \leftarrow r/f$   
10:  end while  
11: end for  
12: if  $r \neq 1$  then  
13:   append  $r$  to  $\mathbf{b}$   
14: end if  
15: return  $\mathbf{b}$ 
```

---

### J.3 Layerwise fitting procedure

The full layerwise fitting procedure is given in Algorithm 3 (Appendix J.3). It iterates over Adam steps, refreshing the quantized codebook target every  $T$  steps to reduce calibration cost.

---

#### Algorithm 3 Layerwise fitting of HARP for a linear layer

---

- Require:** Weight  $W \in \mathbb{R}^{d_{\text{out}} \times d_{\text{in}}}$ , second moment  $H \in \mathbb{R}^{d_{\text{in}} \times d_{\text{in}}}$
- Require:** Blockwise codebook quantizer  $Q(\cdot)$ ; HARP initialization  $\Theta_U = \Theta_V = 0$
- Require:** Adam step size  $\eta$ , steps  $S$ , block size  $g$ , regularizer  $\lambda_{\text{bd}}$ , target refresh interval  $T$  (default  $T = 1$ )
- 1: Initialize  $U(\Theta_U) \in O(d_{\text{out}})$  and  $V(\Theta_V) \in O(d_{\text{in}})$  as HARP processors
  - 2: **for**  $s = 1$  to  $S$  **do**
  - 3:   Compute rotated weights  $\tilde{W} \leftarrow U^\top W V$
  - 4:   Compute rotated second moment  $\tilde{H} \leftarrow V^\top H V$
  - 5:    $\tilde{w}_j \leftarrow |\tilde{H}_{jj}| / \text{mean}(|\tilde{H}_{jj}|)$  and  $\text{stopgrad}(\tilde{w})$
  - 6:   **if**  $s \bmod T = 1$  or  $T = 1$  **then**
  - 7:      $\hat{\tilde{W}} \leftarrow \text{stopgrad}(Q(\tilde{W}))$
  - 8:   **end if**
  - 9:    $\Delta \leftarrow \tilde{W} - \hat{\tilde{W}}$
  - 10:    $\mathcal{L}_{\text{diag}} \leftarrow \frac{1}{d_{\text{out}} d_{\text{in}}} \sum_{i,j} \Delta_{ij}^2 \tilde{w}_j$
  - 11:   Compute  $\mathcal{R}_{\text{bd}}$  from Eq. (15)
  - 12:    $\mathcal{L}_{\text{fit}} \leftarrow \mathcal{L}_{\text{diag}} + \lambda_{\text{bd}} \mathcal{R}_{\text{bd}}$
  - 13:   Update  $\Theta_U, \Theta_V$  with Adam using  $\nabla \mathcal{L}_{\text{fit}}$
  - 14: **end for**
  - 15: Optionally quantize HARP parameters to int8 as in Section 3.5.2
  - 16: **return** Fitted processors  $U, V$
- 

### J.4 Int8 storage of HARP parameters

After fitting, we optionally quantize HARP parameters to 8-bit integers for storage efficiency. For  $b_t > 2$  stages we store only the strict upper triangle of the skew-symmetric matrix  $A(\theta)$ , which has  $b_t(b_t - 1)/2$  entries per block. For  $b_t = 2$  stages we store the single Givens angle. For each block  $c$ , we compute a per-block scale

$$s_{t,c} = \max |a_{t,c}| / 127$$

and store

$$q_{t,c} = \text{round}(a_{t,c} / s_{t,c}).$$

At runtime we reconstruct  $a_{t,c} \approx s_{t,c} q_{t,c}$  and build the corresponding orthogonal block using the Givens or Cayley parameterization.